Available online at www.sciencedirect.com
SCIENCE DIRECT®
International Journal of Thermal Sciences 45 (2006) 138–150
International Journal of Thermal Sciences
www.elsevier.com/locate/ijts

Entropy generation and optimal analysis for laminar forced convection in curved rectangular ducts: A numerical study

T.H. Ko *, K. Ting

Department of Mechanical Engineering, Lunghwa University of Science and Technology, 300, Wan-Shou Rd., Sec. 1, Kueishan, 33306, Taoyuan, Taiwan, ROC

Received 22 October 2004; received in revised form 7 January 2005; accepted 7 January 2005

Available online 9 June 2005

Abstract

The present paper analyzes entropy generation induced by forced convection in a curved rectangular duct with external heating by numerical methods. The problem is assumed as steady, three-dimensional and laminar. The local entropy generation distributions as well as the overall entropy generation in the whole flow fields, including the entrance region and fully developed region, are analyzed. The effects of three important factors, including Dean number, external wall heat flux and cross-sectional aspect ratio, on entropy generated from frictional irreversibility and heat transfer irreversibility are investigated separately in detail. The results show that the major source of entropy generation in the flow fields with larger Dean number and smaller wall heat flux comes from frictional irreversibility; whereas for the flow fields with smaller Dean number and larger wall heat flux the entropy generation is dominated by heat transfer irreversibility. The competition between the entropy generation from the irreversibility caused by fluid friction and heat transfer is complicatedly related with the three factors, making the relationship between the resultant entropy generation and the three factors non-monotonous. Based on the minimal entropy generation principal, the optimal condition can induce the minimal entropy generation in the flow fields. Through the optimal analysis, the optimal aspect ratio is found to be dependent on heat flux and Dean number. For each case with specific aspect ratio and wall heat flux, there exists an optimal Dean number, and the optimal Dean number is found to increase with wall heat flux. The detailed optimal analysis is provided in the present paper, which is worthwhile for heat exchanger design from the second law of thermodynamics since the thermal system could have the least irreversibility and best exergy utilization if the optimal Dean number and aspect ratio can be selected according to the practical design conditions.

Keywords: Curved rectangular duct; Forced convection; Irreversibility; Entropy generation; Exergy; CFD

1. Introduction

Curved ducts extensively occur in many industrial applications, such as air conditioning systems, heat exchangers, and the blade-to-blade passage in modern gas turbines. The most important flow characteristics in curved ducts are the secondary flow structures, which are generated by the curvature effect and centrifugal force. The secondary flow motion increases the heat transfer coefficient, meanwhile it also induces more serious pressure drop in curved ducts. Because of the practical importance, the flow dynamics and heat transfer in curved ducts with different cross-sectional shapes, including circular, rectangular and elliptic, have received continuous attention in past several decades [1–8]. For rectangular cross section, which is the principal interest of the present paper, Cheng et al. [3] analyzed the flow field in a fully developed laminar flow in a curved rectangular channel. Bolinder [4] studied the flow structure in a helical rectangular duct, in which the effects of the curvature and torsion in the flow were emphasized. Wang [5] studied the buoyancy–force–driven transition and its effects on the heat transfer in a rotating curved rectangular channel. Silva et al. [6] carried out the hydrodynamic and thermal analysis of fully developed laminar flow in curved rectangular and elliptic ducts by numerical methods. In their study, a gen-

* Corresponding author. Tel: +886 2 82093211; fax: +886 2 82091475.
E-mail address: thko@mail.lhu.edu.tw (T.H. Ko).

1290-0729/$ – see front matter
doi:10.1016/j.ijthermalsci.2005.01.010

Nomenclature

a	width of the cross-sectional area of rectangular curved duct ..... m	S'''_P	volumetric entropy generation rate due to friction ..... $W\cdot m^{-3}\cdot K^{-1}$
b	height of the cross-sectional area of rectangular curved duct ..... m	S'''_T	volumetric entropy generation rate due to heat transfer ..... $W\cdot m^{-3}\cdot K^{-1}$
Be	Bejan number	S'''_{gen}	total volumetric entropy generation rate ..... $W\cdot m^{-3}\cdot K^{-1}$
d_e	hydraulic diameter ..... m	S^*_P	non-dimensional entropy generation rate due to friction
De	Dean number, $= Re(d_e/r_c)^{1/2}$	S^*_T	non-dimensional entropy generation rate due to heat transfer
$\bar{h}$	average heat transfer coefficient in the rectangular curved duct ..... $W\cdot m^{-2}\cdot K^{-1}$	S^*_{gen}	non-dimensional entropy generation rate
k	thermal conductivity ..... $W\cdot m^{-1}\cdot K^{-1}$	T	temperature ..... K
Nu	Nusselt number, $= \bar{h}d_e/k$	T_0	temperature at duct entrance ..... K
P	pressure ..... Pa	V	average velocity in duct ..... $m\cdot s^{-1}$
q''	wall heat flux ..... $W\cdot m^{-2}$	μ	molecular viscosity ..... $kg\cdot m^{-1}\cdot s^{-1}$
q^*	non-dimensional heat flux	ρ	density ..... $kg\cdot m^{-3}$
$\dot{Q}$	heat transfer rate ..... W	γ	aspect ratio
R	gas constant ..... $J\cdot kg^{-1}\cdot K^{-1}$	ϕ	irreversibility distribution ratio
Re	Reynolds number		
r_c	radius of curvature ..... m		

eral correlation of Nusselt number and friction factor as a function of Dean number (De) and the cross-sectional aspect ratio of the duct were proposed. Chandratilleke [7] used experimental method, and Chandratilleke and Nursubyakto [8] used both of numerical and experimental methods to investigate the secondary flow and convective heat transfer in curved rectangular ducts with external heating, in which the effects of Dean number and duct aspect ratio on the heat transfer coefficient and flow fields are analyzed.

As a good heat-exchanger passage, the curved duct should provide the most effective heat transfer performance and the least friction loss so that the available energy can be utilized efficiently. However, the heat transfer enhancement in a thermal system is always achieved at the expense of the increase of friction loss. Such inevitable conflict makes the optimal trade-off by selecting the most appropriate configuration and the best flow conditions become the critical challenge for the design work. Recently, entropy generation has been used as an index for evaluating the significance of irreversibility related to heat transfer and friction in a thermal system. Based on the concept of efficient exergy use and minimal entropy generation principal, optimal designs of thermodynamic systems have been widely proposed from the viewpoint of thermodynamic second law [9–18]. Bejan [10] has described the systematic methodology of computing entropy generation through heat and fluid flow in several heat exchangers. Nag and Kumar [11] studied the optimization from second law for convective heat transfer through a duct with constant heat flux. Sahin [12] performed the irreversibility analysis in various duct geometries with constant wall heat flux and laminar flow. Sahin [13] investigated the entropy generation and pumping power in a turbulent fluid flow through a smooth pipe subjected to constant heat flux. Shuja [14] proposed the optimal fin geometry in an electronics cooling system based on the exergoeconomic analysis. Sara et al. [15] performed the second law analysis of rectangular channels with square pin-fins. In the recent researches of Ko and Ting [16,17] and Ko et al. [18], the work for optimizing the helical coils by using the minimal entropy generation concept has been carried out, in which the optimal Reynolds number of the helical coils have been presented.

Similar with other thermal systems, the forced convection in curved rectangular ducts also faces the challenge of inventing the optimal design to have the minimal entropy generation. However, most of the previous investigations on curved rectangular ducts are restricted to the analysis based on the first law of thermodynamics, whereas very rare exergy analysis has been addressed. The aim of the present paper is to investigate the entropy generation due to laminar forced convection in curved rectangular ducts with constant wall heat flux. The influences of external heat flux, Dean number and cross-sectional aspect ratio on the entropy generation will be emphasized, through which the optimal Dean number and aspect ratio according to the relevant design parameters to induce the best exergy utilization with the minimal entropy generation and least irreversibility will be discussed.

2. Physical model

Fig. 1 shows the semi-circular curved rectangular duct analyzed in the present paper. The side lengths of the cross-section are a and b, respectively; the aspect ratio, γ, is defined as b/a. The Reynolds number (Re), Nusselt number

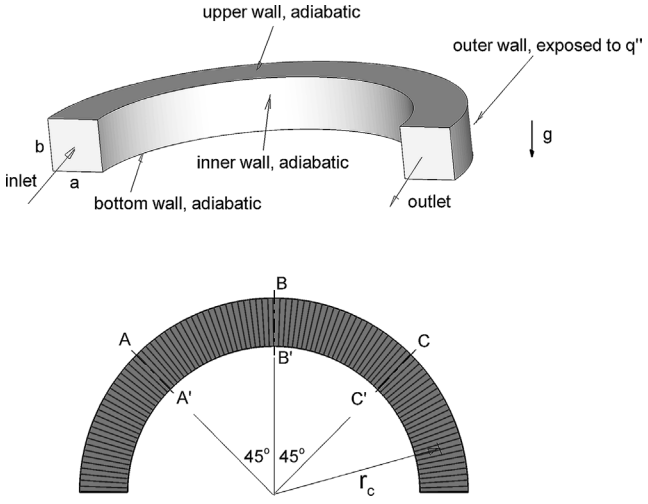

Fig. 1. Geometry and coordinate system of a curved rectangular duct.

(*Nu*) and Dean number (*De*) for the current problem are defined as follows:

$$Re = \rho V d_e/\mu \tag{1}$$

$$Nu = \bar{h} d_e/k \tag{2}$$

and

$$De = Re(d_e/r_c)^{1/2} \tag{3}$$

where V and $\bar{h}$ are the average velocity and average heat transfer coefficient of the flow in the curved duct; d_e is the characteristic length defined as $2ab/(a+b)$; r_c is the curvature radius of the curved duct. Air has been selected as working fluid in the present study. Due to the small temperature change in the flow field, the thermophysical properties of molecular viscosity (μ) and thermal conductivity (k) are assumed to be constant as 1.846×10^{-5} kg·m^{-1}·s^{-1} and 0.0263 W·m^{-1}·K^{-1}, respectively. The buoyancy force due to gravity has been included in consideration. The fluid density at duct entrance is 1.161 kg·m^{-3}. The calculated cases cover three aspect ratios, $\gamma = 0.5$, 1.0 and 2.0; and *De* ranging from 100 to 5000. The non-dimensional wall heat flux, q^*, is defined according to the external wall heat flux, q'', as

$$q^* = q''\sqrt{ab}/kT_0 \tag{4}$$

where T_0 is the fluid temperature at duct entrance. Four heat flux cases, including $q^* = 0.112$, 0.224, 0.448 and 0.896, are analyzed. For ensuring the studied cases are laminar flows, the critical *Re* for the rectangular curved duct flow must be checked. However, rare information directly indicates the critical *Re* for a rectangular curved duct flow in open publications. Nonetheless, the critical *Re* for helical pipe flows has been reported by several researches [19,20]. According to the study of Srinivasan [19], the critical *Re* for helical pipe flows, which determines the flow is laminar or turbulent, is related with the coil curvature ratio, δ, which is defined by the ratio of coiled tube radius to the curvature radius. The relationship is:

$$Re_{\text{crit}} = 2100\left(1 + 12\delta^{1/2}\right) \tag{5}$$

which indicates Re_{crit} increases with δ. For the rectangular cross-section in present problems, the curvature ratio is calculated by the ratio of characteristic length, i.e. $\delta = d_e/r_c$. The minimal curvature ratio in the present calculated cases is 0.267. According to the report of Srinivasan [19], the critical *Re* is 15121. In addition, the study of Mishra and Gupta [20] pointed out the critical *Re* for helical coil flows will increase as the coil pitch decreases. For the curved duct investigated in present paper, the pitch is identical zero; therefore, the critical *Re* for the current problems should be larger than the magnitude calculated from the expression of Srinivasan [19]. Since the focus is on laminar flows, the range of studied *De* in present paper is limited between 100 and 5000, and the corresponding *Re* is between 194 and 9676, which is much lower than the critical *Re* to ensure the flows are laminar.

3. Mathematical model and numerical method

3.1. Mathematical model

The present problem is assumed as three-dimensional, laminar and steady. The continuity equation, Navier–Stokes equation, energy equation and equation of state are solved simultaneously. The equations in tensor form are as follows:

$$\frac{\partial(\rho U_i)}{\partial x_i} = 0 \tag{6}$$

$$\frac{\partial}{\partial x_j}(\rho U_j U_i) = -\frac{\partial P}{\partial x_i} + \frac{\partial}{\partial x_j}\left[\mu\left(\frac{\partial U_i}{\partial x_j} + \frac{\partial U_j}{\partial x_i}\right) - \frac{2}{3}\mu\frac{\partial U_k}{\partial x_k}\delta_{ij}\right] + \rho g_i \tag{7}$$

$$\frac{\partial}{\partial x_j}\left(\rho U_j C_p T - k\frac{\partial T}{\partial x_j}\right) = U_j\frac{\partial P}{\partial x_j} + \left[\mu\left(\frac{\partial U_i}{\partial x_j} + \frac{\partial U_j}{\partial x_i}\right) - \frac{2}{3}\mu\frac{\partial U_k}{\partial x_k}\delta_{ij}\right]\frac{\partial U_i}{\partial x_j} \tag{8}$$

$$P = \rho RT \tag{9}$$

The boundary conditions are considered as below. At inlet, only the axial velocity component is non-zero, and the velocity distribution is assumed to be uniform. At outlet, the diffusion flux in the direction perpendicular to the outlet plane for all velocity components and T are set to zero. For ensuring the outlet boundary condition is appropriate, a straight section with length $10d_e$ has been added at the end of the curved duct, and the zero flux condition was applied at the end of the straight section. By comparing the flow fields in the curved duct part from the calculated results of the cases with or without the extra straight section, no evident difference was detected. Non-slip conditions are specified on all solid walls. As shown in Fig. 1, the constant heat flux is specified only on the outer wall, whereas on other walls adiabatic condition is applied.

After the velocity and temperature distributions of the flow field are solved by using Eqs. (6)–(9) and the accompanied boundary conditions, the volumetric entropy generation

due to the heat transfer irreversibility (S'''_T) and the fluid frictional irreversibility (S'''_P) can be calculated by the following equations [10]:

$$S'''_T = \frac{k}{T^2}\left(|\nabla T|\right)^2 \tag{10}$$

$$S'''_p = \frac{\mu}{T}\left(\frac{\partial U_i}{\partial x_j} + \frac{\partial U_j}{\partial x_i}\right)\frac{\partial U_i}{\partial x_j} \tag{11}$$

The total volumetric entropy generation in the flow field can be obtained by

$$S'''_{\text{gen}} = S'''_T + S'''_P \tag{12}$$

According to Bejan [10], the ratio of S'''_P and S'''_T is defined as the irreversibility distribution ratio, ϕ:

$$\phi = S'''_P / S'''_T \tag{13}$$

Paoletti et al. [21] proposed an alternative irreversibility distribution parameter, Bejan number (*Be*), to describe the contribution of heat transfer entropy on overall entropy generation. The Bejan number is defined as

$$Be = S'''_T / S'''_{\text{gen}} \tag{14}$$

The *Be* ranges from 0 to 1. Accordingly, $Be = 0$ and $Be = 1$ are two limiting cases representing the irreversibility is dominated by fluid friction and heat transfer, respectively. When $Be = 0.5$, the entropy generation rates from heat transfer and fluid friction are equal.

3.2. Numerical method

All the above-mentioned equations accompanied with boundary conditions are discretized by a finite volume formulation. In the equations, the convective terms are modeled by the secondary-order upwind scheme; meanwhile the diffusive terms are modeled by the central difference scheme. The numerical solution procedure adopts the well-known semi-implicit SIMPLE algorithm, which was developed by Launder and Spalding [22]. All the detailed numerical procedure can be found in the book of Patankar [23]. The convergent criteria is set as the relative residual of all variables, including the mass, all velocity components and temperature less than 10^{-4}. The results have been compared with those from the calculation with the convergent criteria set as 10^{-6}, and the results are almost the same. A commercial CFD software CFD RC (ESI US R&D, Inc.) is used for the numerical solutions.

4. Results and discussion

4.1. Grid independent test and code validation

For grid independent test, three uniform spacing grid systems with, including 45 000, 80 000 and 200 000 cells, are adopted to calculate a baseline case. Fig. 2 shows the Nusselt number at fully developed condition for the case calculated

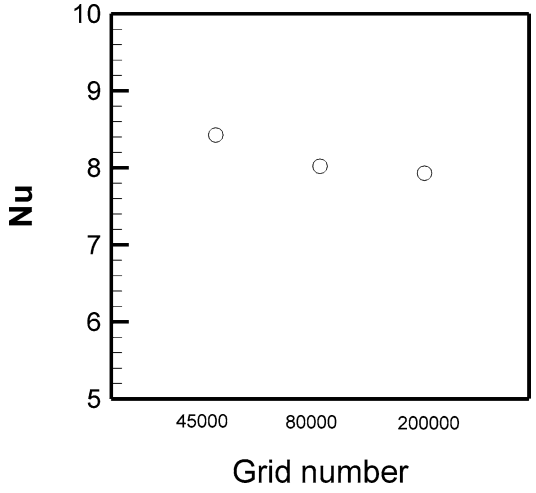

Fig. 2. Predicted Nusselt number at fully developed condition by different grid systems.

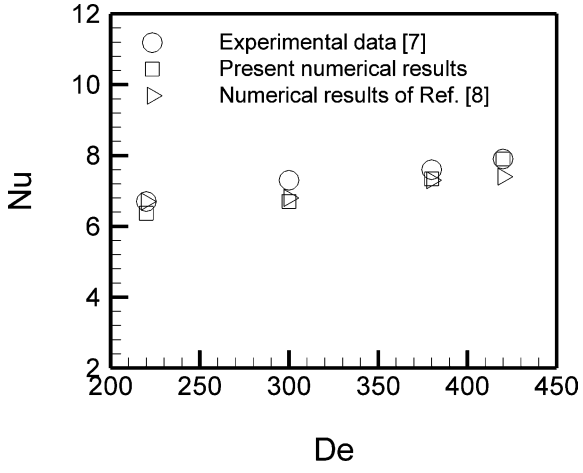

Fig. 3. Comparison of predicted Nusselt number at fully developed condition with experimental data [7] and numerical results of Chandratilleke and Nursubyakto [8].

by the three grid systems, from which the difference between the results of 80 000 and 200 000 cells are found to be very limited. Therefore, 80 000 cells are concluded as dense enough to get the grid independent solutions. In the following cases, the grid system with 80 000 cells is used.

For validating the accuracy of numerical solutions, the Nusselt number under fully developed condition from current numerical solutions are compared with the experimental data of Chandratilleke [7] and the numerical results by Chandratilleke and Nursubyakto [8]. The aspect ratio and the wall heat flux of the compared case are 2 and 25 $\text{W}\cdot\text{m}^{-2}$, respectively. The comparisons, as shown in Fig. 3, cover four cases of $De = 220$, 300, 380 and 420. For all the compared cases, the deviation between the present numerical results and the experimental data of Chandratilleke [7] or the numerical results by Chandratilleke and Nursubyakto [8] is very limited. Only relatively larger deviation occurs in $De = 300$ cases. The largest deviation is only about 8.2%. Therefore, the

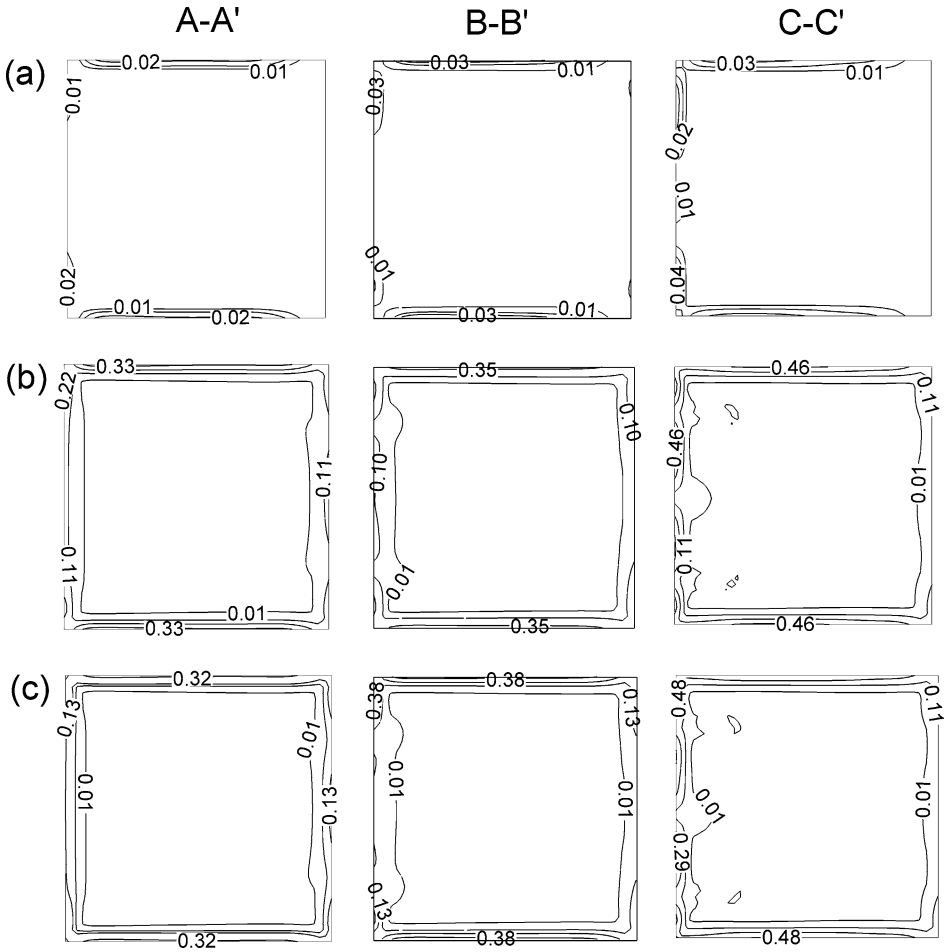

Fig. 4. The contours of volumetric entropy generation, S'''_P, on cross-sectional planes at A–A', B–B' and C–C' for $\gamma = 1$ case, (a) $q^* = 0.224$, $De = 1000$; (b) $q^* = 0.224$, $De = 3000$; and (c) $q^* = 0.896$, $De = 3000$. On each cross-sectional plane, outer wall is at left-hand side, inner wall is at right-hand side.

present numerical predictions are verified to have reasonable accuracy.

4.2. Local distributions of entropy generation for baseline cases with $\gamma = 1$

For understanding the development of entropy generation in the curved duct, the distribution of volumetric entropy generation, S'''_P, S'''_T and S'''_{gen}, on cross-sectional planes at A–A', B–B' and C–C' (see Fig. 1) for three baseline cases of $\gamma = 1$ with $q^* = 0.224$, $De = 1000$; $q^* = 0.224$, $De = 3000$; and $q^* = 0.896$, $De = 3000$ are studied first. Figs. 4(a)–(c) show the distributions of S'''_P for the three cases, respectively. In the figures, the outer wall, which is exposed to the external heating, is on the left-hand side of the cross-section, and the right-hand side wall of the cross-section is inner wall. The significant S'''_P appears only in the limited region adjacent to the duct walls because of the serious velocity gradient in the region. Besides, S'''_P in the regions near the upper and lower walls is found to be larger than that in the region near the inner and outer walls. As the flow develops from A–A' to C–C', the distributions of S'''_P have no great change, but the magnitudes of S'''_P keeps increasing mildly along downstream. By comparing Figs. 4(a) and (b), the increase of De tends to cause the increase of S'''_P, which is attributed to the more serious fluid friction and the accompanied frictional irreversibility induced by the larger De. However, the effects of q^* on S'''_P, which can be detected through the comparison between Figs. 4(b) and (c), are relatively minor. According to the calculated results, the maximum temperature rise in case of $q^* = 0.896$ and $De = 3000$ is only about 16 K, which is less than 6% of the initial fluid temperature at entrance. The limited difference of temperature makes the change of principal velocity distribution and velocity gradient be insignificant, and therefore yields the similar S'''_P distribution in different q^* cases. The distributions of S'''_T for the same three cases are shown in Figs. 5(a)–(c). The significant S'''_T concentrates near the outer wall exposed to the external heating, whereas S'''_T is very minor in the central core of the duct and the region near the inner wall. As flow develops along downstream, the region with large S'''_T gradually penetrates toward the central core of the duct. When comparing Figs. 5(a) and (b), the increase of De is found to induce the decrease of S'''_T, which is attributed to that the increase of De will result the increase of heat transfer coefficient, and in turn makes the tempera-

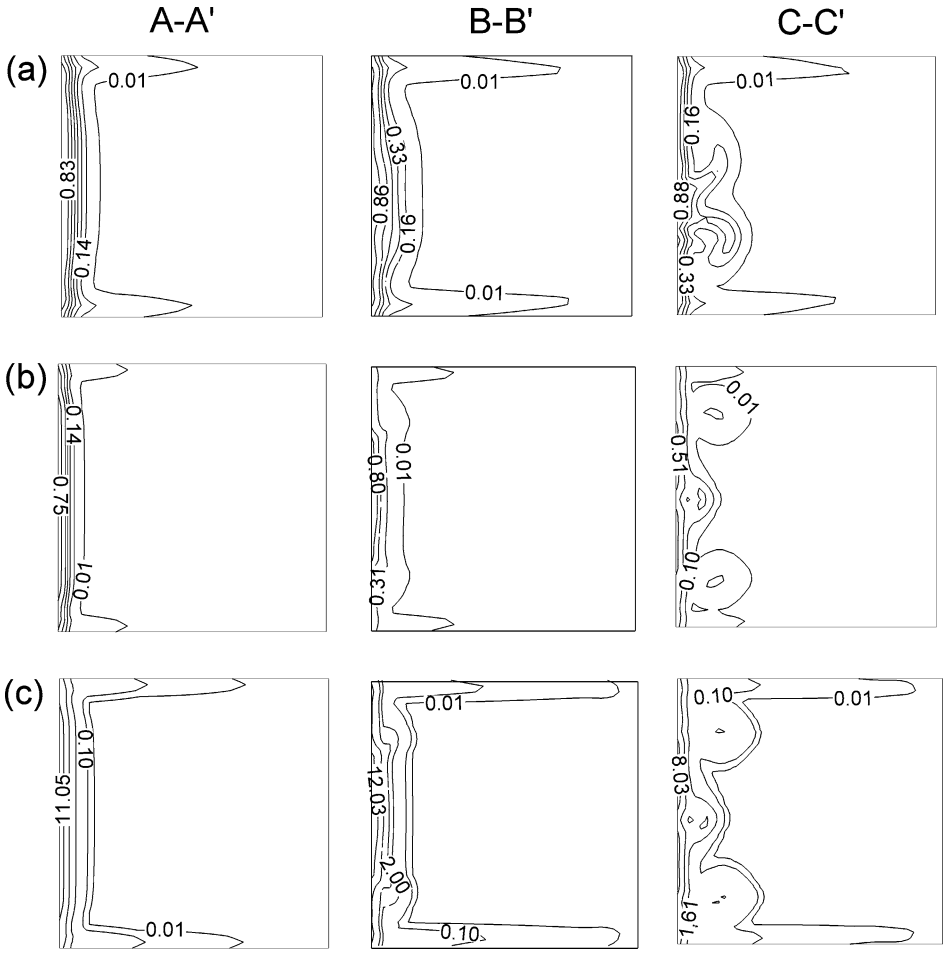

Fig. 5. The contours of volumetric entropy generation, S'''_T, on cross-sectional planes at A–A', B–B' and C–C' for $\gamma = 1$ case, (a) $q^* = 0.224$, $De = 1000$; (b) $q^* = 0.224$, $De = 3000$; and (c) $q^* = 0.896$, $De = 3000$. On each cross-sectional plane, outer wall is at left-hand side, inner wall is at right-hand side.

ture distribution become smoother, and reduces the entropy generation, S'''_T. Since the increase of q^* causes more heat transfer irreversibility in the flow field, the magnitudes of S'''_T are raised obviously in the larger q^* case, which can be clearly found through the comparison of Figs. 5(b) and (c).

The distribution of resultant entropy generation, S'''_{gen} for the three cases is shown in Figs. 6(a)–(c). The principal entropy generation occurs within a thin layer near the duct walls, and the largest S'''_{gen} concentrates in regions adjacent to the outer wall exposed to external heating, whereas the entropy generation is very minor in central core of the duct, which indicates the major source of entropy generation in the flow fields comes from the near wall region where the temperature and velocity gradients are most significant. As the flow develops along downstream, from A–A' to C–C', the layer with large entropy generation gradually penetrates toward the central core from the heated outer wall, but the penetrated depth is still limited. The influences of De on entropy generation can be investigated through the comparison of Figs. 6(a) and (b). An obvious difference is that there is almost no significant entropy generation occurring in the region near the inner wall for $De = 1000$ case, but the entropy generation becomes evident in the same region while De increases to 3000. The comparison also indicates the increase of De tends to cause the reduction of entropy generation in the region near the heated outer wall. In $De = 3000$ case, the layer with large entropy generation near the heated outer wall is found to become thinner when compared with $De = 1000$ case. The different influences of De on the entropy generation in the regions near outer heated wall and inner wall are attributed to the opposite influences of De on entropy generation from frictional irreversibility and that from heat transfer irreversibility. As described in Eq. (12), entropy can be generated from the irreversibility of fluid friction and the heat transfer. When De increases, both of the fluid friction and heat transfer coefficient will increase. As discussed previously, the increase of fluid friction results the increase of entropy generation, S'''_P, whereas the increase of heat transfer coefficient makes the temperature distribution become smoother, and in turn reduces the entropy generation, S'''_T. The competition of S'''_P and S'''_T in the flow fields, which is dependent on the flow regions, determines the final changes of the resultant entropy generation, S'''_{gen}. Figs. 7(a)–(c) show the Be contours on cross-sectional planes at A–A', B–B' and C–C' for the three cases. Near the heated wall region, Be is greater than 0.5 for all cases,

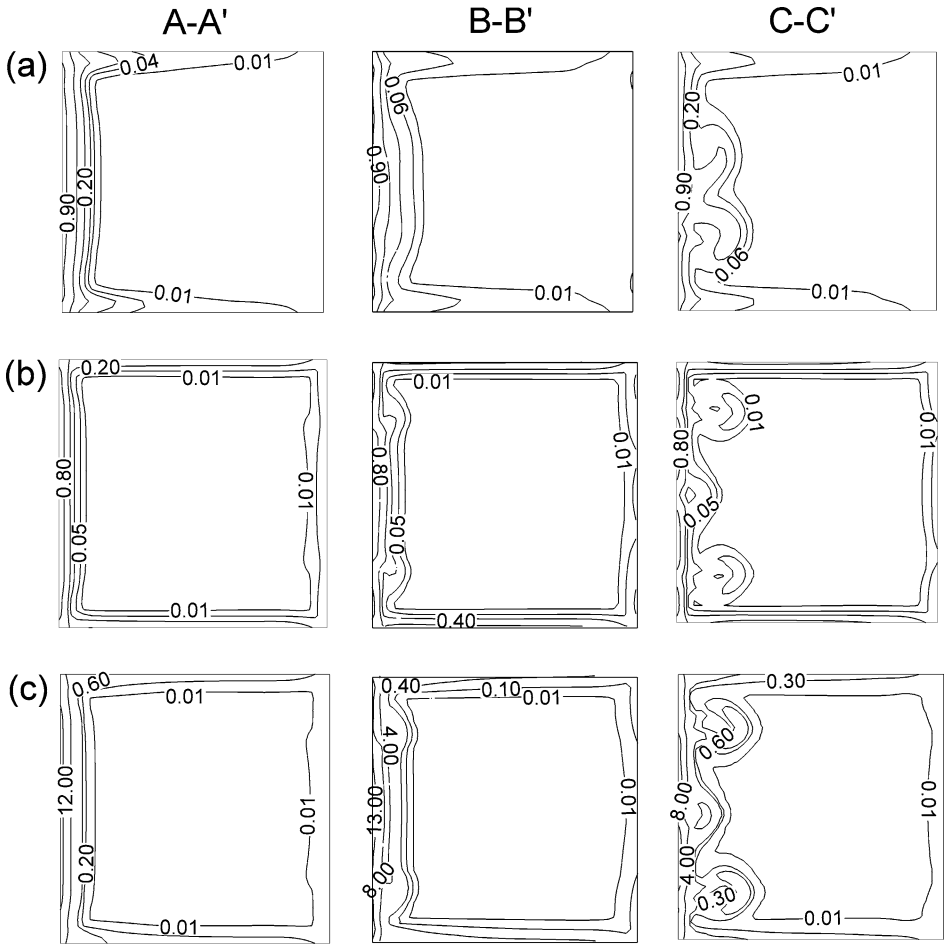

Fig. 6. The contours of volumetric entropy generation, S'''_{gen}, on cross-sectional planes at A–A', B–B' and C–C' for $\gamma = 1$ case, (a) $q^* = 0.224$, $De = 1000$; (b) $q^* = 0.224$, $De = 3000$; and (c) $q^* = 0.896$, $De = 3000$. On each cross-sectional plane, outer wall is at left-hand side, inner wall is at right-hand side.

which reveals the entropy generation in the region is dominated by the heat transfer irreversibility. As flow develops from A–A' to C–C', the region with Be greater than 0.5 penetrates toward the central core region gradually, and the magnitude of Be keeps increasing in the whole region. The results are attributed to the more and more heat is transferred into the flow field from the heated outer wall as flows develop along downstream. However, near the inner wall, Be is always less than 0.5, which indicates the major entropy generation in the region comes from the frictional irreversibility rather than heat transfer. The influences of De on Be can be detected from the comparison between Figs. 7(a) and (b). Clearly, as De increases from 1000 to 3000, the magnitudes of Be in the whole domain are found to decrease, and the region with Be less than 0.5 becomes much wider in $De = 3000$ case, which reflects the results that the increase of De causes enhancement of heat transfer, and in turn makes temperature gradient and S'''_T become mild; meanwhile the larger De causes more serious fluid friction, and thus increases the frictional irreversibility and S'''_P. Besides, Be becomes much smaller than 0.5 in the region adjacent to inner wall as De increases, which indicates S'''_P becomes much larger than S'''_T in the region. The above information indicating the entropy generation near the heated wall is dominated by S'''_T and the increase of De tends to reduce the magnitude, gives the explanations why S'''_{gen} near the heated wall decreases with the increase of De as previous discussion based on Figs. 6(a) and (b). Meanwhile, since the entropy generation in the region near the inner wall is dominated by S'''_P, and its magnitude is raised by the more serious frictional irreversibility in larger De cases, the entropy generation becomes more evident in the region near inner wall in the larger De cases, which again verifies the previous discussion based on the comparison of Figs. 6(a) and (b).

The influences of heat flux on entropy generation can be studied from the comparison of Figs. 6(b) and (c). Clearly, the increase of heat flux is found to cause the increase of entropy generation in whole flow fields because of the more serious irreversibility due to the larger heat transfer. When comparing Figs. 7(b) and (c), the larger heat flux is found to cause the increase of Be. Especially in the region near the heated wall where the external heating is directly imposed, the magnitudes of S'''_{gen} and Be increase considerably in the larger q^* case.

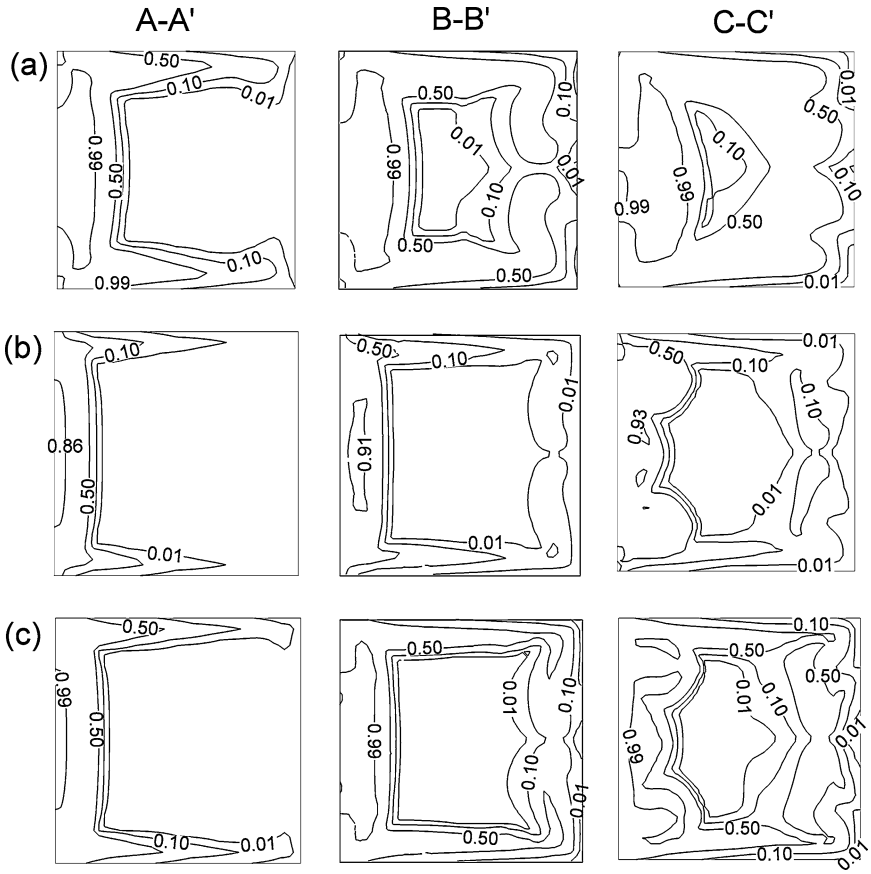

Fig. 7. The contours of *Be* on cross-sectional planes at A–A', B–B' and C–C' for $\gamma = 1$ case, (a) $q^* = 0.224$, $De = 1000$; (b) $q^* = 0.224$, $De = 3000$; and (c) $q^* = 0.896$, $De = 3000$. On each cross-sectional plane, outer wall is at left-hand side, inner wall is at right-hand side.

4.3. Effects of De and q^* on S_P^* and S_T^* for $\gamma = 1$ case

For fair evaluation of the entropy generation in the flow fields with different external wall heat flux, the non-dimensional entropy generation rate, S_P^*, S_T^* and S_{gen}^*, in the whole curved duct are defined by

$$S_P^* = \frac{\int_V S_P''' \, \mathrm{d}V}{\dot{Q}/T_0} \tag{15}$$

$$S_T^* = \frac{\int_V S_T''' \, \mathrm{d}V}{\dot{Q}/T_0} \tag{16}$$

and

$$S_{\text{gen}}^* = \frac{\int_V S_{\text{gen}}''' \, \mathrm{d}V}{\dot{Q}/T_0} \tag{17}$$

where V is the total volume of the computational domain; $\dot{Q}$ is the heat flow rate into the flow field. The relationship between the entropy generation and *De* for different heat flux cases is shown in Fig. 8. A clear trend can be found from the figure that S_P^* increases and S_T^* decreases as *De* increases for all heat flux cases. As discussed previously, the increase of S_P^* with the increase of *De* is caused by the more serious frictional irreversibility in larger *De* cases, whereas the reduction of S_T^* in larger *De* cases is attributed to that the heat transfer coefficient is enhanced by the larger *De* and thus results the milder temperature gradient in the flow field. Besides, the increase of heat flux is found to cause S_P^* to decrease and S_T^* to increase. Since the temperature rise in the flow field is minor, the principal velocity distributions are only slightly affected by heat flux; therefore, the magnitudes of velocity gradient in cases with different heat flux do not have great change. However, because the temperature term appears in the denominator of S_P''', as shown in Eq. (11), and S_P^* is the normalization of S_P''' by $\dot{Q}/T_0$, the resultant S_P^* is induced to become smaller in the larger q^* cases. Meanwhile, the more serious heat transfer irreversibility is caused by the larger q^*, and thus S_T^* is induced to increase with q^* for all *De* cases. The competition between the magnitudes of S_P^* and S_T^*, which is also indicated in Fig. 8, can be found to be dependent on *De* and q^*. For $q^* = 0.112$, 0.224 and 0.448 cases, S_P^* and S_T^* curves intersect each other at $De = 1750$, 2835 and 4688, respectively. For the cases with *De* less than the intersectional *De*, S_T^* is larger than S_P^*, and *vice verse* when *De* exceeds the intersectional *De*. Through the comparison between the three q^* cases, the *De* range where S_T^* is larger than S_P^*, becomes wider as q^* increases. As for $q^* = 0.896$ cases, S_T^* keeps as larger than S_P^* in all *De* cases. These results provide worthy information for understanding the major source of entropy generation in different cases with various *De* and heat flux. For cases with high *De*

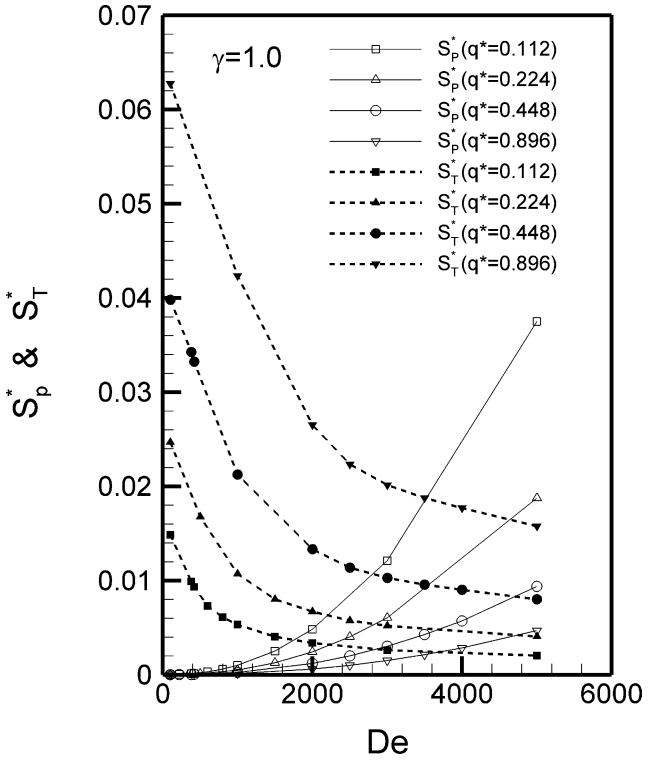

Fig. 8. The effects of *De* on entropy generation induced from heat transfer (S_T^*) and fluid friction (S_P^*) for $\gamma = 1$ case.

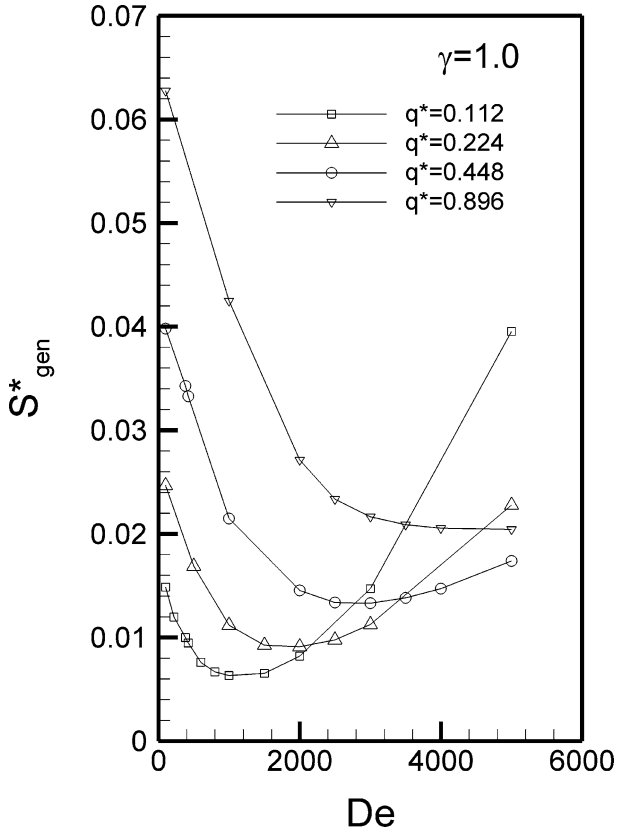

Fig. 9. The relationship between entropy generation, S_{gen}^*, and *De* for $\gamma = 1$ with different q'' values.

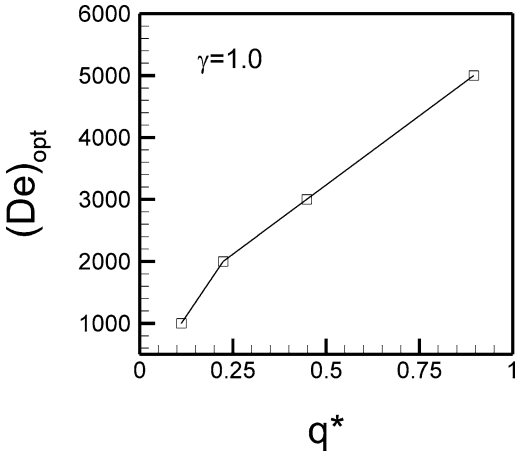

Fig. 10. The optimal *De* for $\gamma = 1$ cases with different q^* values.

and small q^*, S_P^* is the dominant source of entropy generation in the flow fields, whereas the dominant source turns to be S_T^* for cases with low *De* and large q^*.

4.4. Effects of De on S_{gen}^* and optimal De analysis for $\gamma = 1$ case

Fig. 9 shows the relationship between S_{gen}^* and *De* for different q^* cases. The figure indicates clearly S_{gen}^* is not monotonically related with q^* and *De*. For smaller *De* cases ($De < 2179$), S_{gen}^* is largest in $q^* = 0.896$ and smallest in $q^* = 0.112$ case, which is attributed to that S_T^* is the dominant term in smaller *De* cases and it increases with q^*. For larger *De* cases ($De > 3472$), S_{gen}^* is largest in $q^* = 0.112$ case, which is resulted from that S_P^* is the dominant term and it is larger in the smaller q^* cases. However, because of the complex competition of S_P^* and S_T^*, the resultant S_{gen}^* is minimal in $q^* = 0.448$ case, which is neither the largest nor smallest q^* considered in the current studied cases. In the medium *De* ($2179 < De < 3472$) cases, the relationship between S_{gen}^* and q^* is not monotonic either. The minimal S_{gen}^* occurs in $q^* = 0.224$ case. Nonetheless, for every q^* case there exists an optimal *De* with the minimal S_{gen}^*, and the optimal *De* is found to increase with q^*. Fig. 10 shows the optimal *De* for different q^* cases. For quantitative results, the optimal *De* for $q^* = 0.112$, 0.224, 0.448 and 0.896 cases are 1000, 2000, 3000 and 5000, respectively.

4.5. Effects of aspect ratio

For investigating the effect of aspect ratio on the entropy generation, two additional aspect ratio cases, including $\gamma = 0.5$ and $\gamma = 2.0$, with $q^* = 0.224$, $De = 3000$ are calculated. The two additional aspect ratio cases have different side length, but the cross-sectional area and duct volume are the same with $\gamma = 1$ case, which has been discussed previously. Figs. 11(a) and (b) show the contours of volumetric entropy generation, S_{gen}''', on cross-sectional planes at A–A',

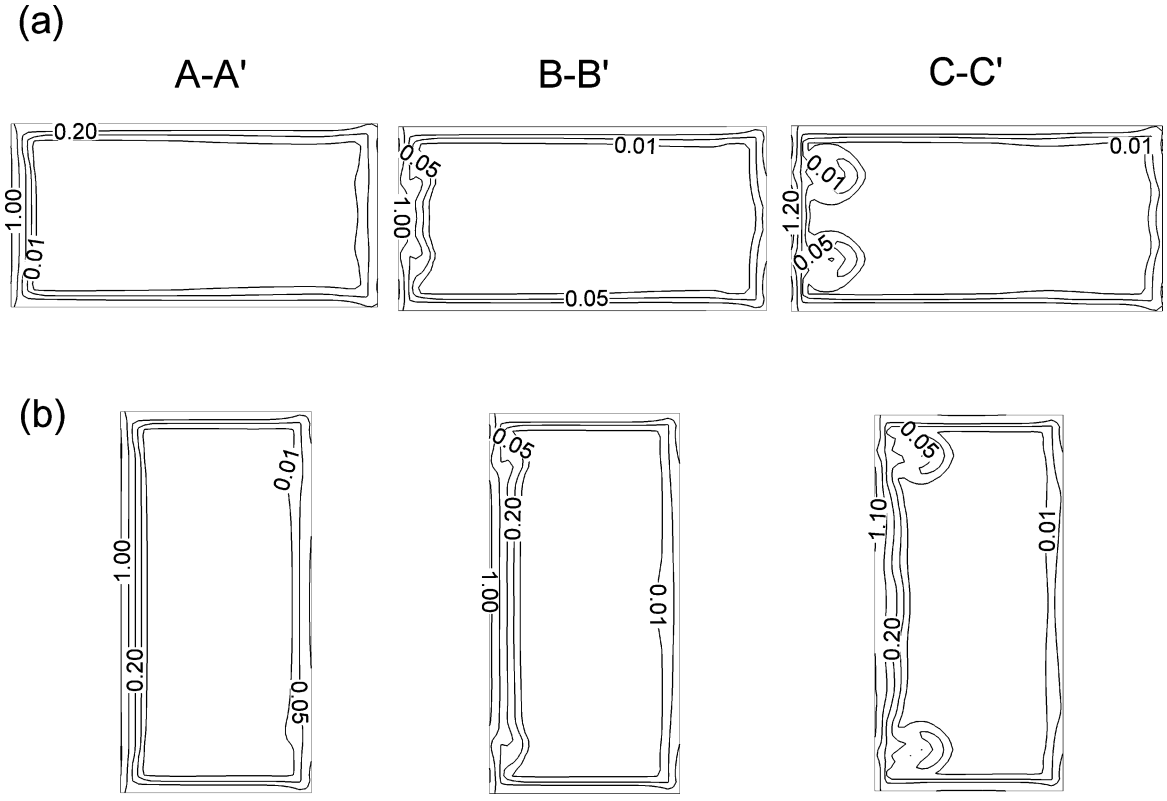

Fig. 11. The contours of volumetric entropy generation, S'''_{gen}, on cross-sectional planes at A–A', B–B' and C–C' for cases of $q^* = 0.224$, $De = 3000$, (a) $\gamma = 0.5$, (b) $\gamma = 2.0$. On each cross-sectional plane, outer wall is at left-hand side, inner wall is at right-hand side.

B–B' and C–C' for the two cases. Similar with the results of $\gamma = 1.0$ case, which has been shown in Fig. 6(b), the distribution with larger S'''_{gen} concentrates near a thin layer near the heated outer wall, and gradually penetrates toward the central core as develops from A–A' to C–C' planes. The magnitudes of S'''_{gen} are comparative for the three aspect ratio cases, but the local maximum of S'''_{gen} is largest in $\gamma = 0.5$ case. Figs. 12(a) and (b) show the distribution of *Be* on cross-sectional planes at A–A', B–B' and C–C' for the two cases. For most regions except the zone near the heated outer wall, *Be* is less than 0.5. The region with *Be* greater than 0.5 concentrates in the region near the heated outer wall, indicating the dominant entropy generation comes from the heat transfer irreversibility; meanwhile *Be* is very small in the region near the inner wall, indicating the entropy generation due to frictional irreversibility is the major source of S'''_{gen} in the region. Besides, through the comparison of Figs. 12(a), (b) and Fig. 7(b), the magnitude of *Be* is largest in $\gamma = 1$ case, which indicates the entropy generation from heat transfer irreversibility is most serious in the case.

Fig. 13 shows the influences of *De* on S^*_P and S^*_T for different aspect ratio cases with $q^* = 0.112$, 0.224, 0.448 and 0.896. As q^* increases, a clear trend can be found from the figure that S^*_P gradually decreases and S^*_T increases for all cases with various γ and *De*. The situation that the entropy generation in the cases with high *De* and small q^* is dominated by S^*_P; whereas the entropy generation in cases with low *De* and large q^* is the dominant by S^*_T, remains the same for all aspect ratio cases as discussed previously. Besides, another important information revealed from Fig. 13 is that for all *De* cases with different q^*, S^*_P is found to be minimal in $\gamma = 2$ case, whereas S^*_T is minimal in either $\gamma = 0.5$ or $\gamma = 2$ case according to *De*, thus making the final evaluation of the aspect ratio requires the further check on the resultant entropy generation, S^*_{gen}. Fig. 14 shows the relationship between S^*_{gen} and *De* for different γ cases with $q^* = 0.112$, 0.224, 0.448 and 0.896. The largest S^*_{gen} is found to appear in the higher *De* side for $q^* = 0.112$ and 0.224 cases, whereas the largest S^*_{gen} location gradually transfers toward the lower *De* side as q^* increases to 0.448 and 0.896. Such developments reveal the fact that S^*_P is the major source of S^*_{gen} for smaller q^* case, so that the greatest S^*_{gen} will appear in the higher *De* side since the higher *De* will cause more serious frictional irreversibility and the resultant S^*_P. For larger q^* case, the dominant entropy generation becomes S^*_T, which results the transfer of the largest S^*_{gen} toward the low *De* region since the low *De* will induce low heat transfer coefficient and cause serious temperature gradient and the corresponding entropy generation, S^*_T. In addition, Fig. 14 also provides the information about the effects of aspect ratio on S^*_{gen}, from which the optimal aspect ratio, γ_{opt}, with the minimal induced S^*_{gen} can be obtained. The optimal aspect ratio is found to be dependent on *De* and q^*, which is analyzed and shown in Table 1.

For every case with specific aspect ratio and heat flux, there exists an optimal Dean number with minimal entropy

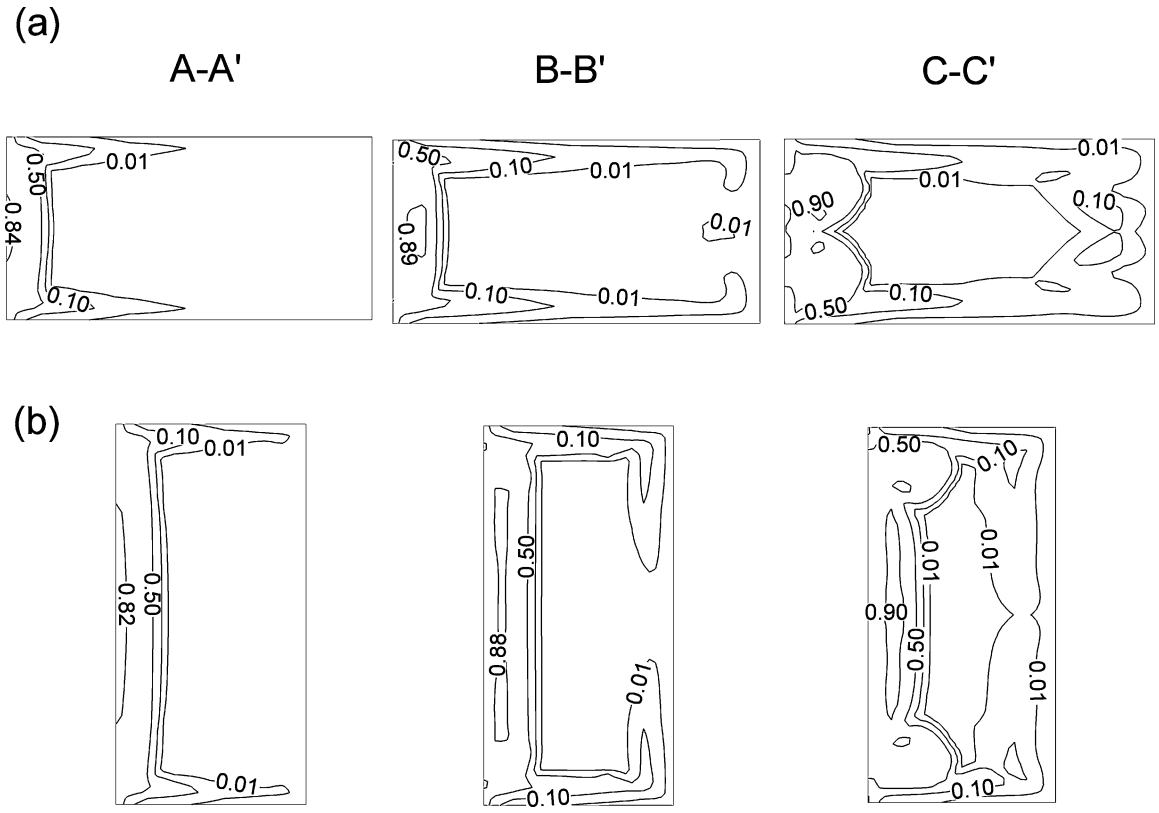

Fig. 12. The contours of Be on cross-sectional planes at A–A', B–B' and C–C' for cases of $q^* = 0.224$, $De = 3000$, (a) $\gamma = 0.5$, (b) $\gamma = 2.0$. On each cross-sectional plane, outer wall is at left-hand side, inner wall is at right-hand side.

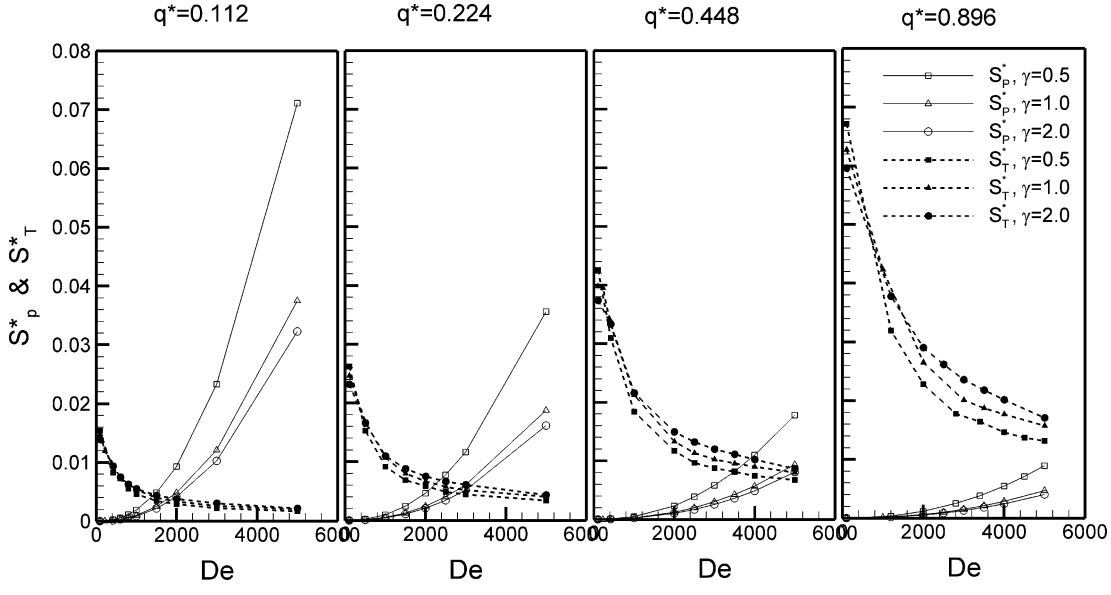

Fig. 13. The effects of De on S_P^* and S_T^* for different aspect ratio cases with various q^*.

generation. Fig. 15 shows the relationship between optimal De and γ for cases with different q^*, from which the optimal De is found to increase as q^* increases. These results provide important information for the heat exchanger design since the optimal De and optimal aspect ratio are suggested to be used according to the practical design conditions so that the thermal system could have the least irreversibility and the best exergy utilization.

5. Conclusions

The entropy generation in a curved duct with various De and q^* is investigated by numerical methods. For lo-

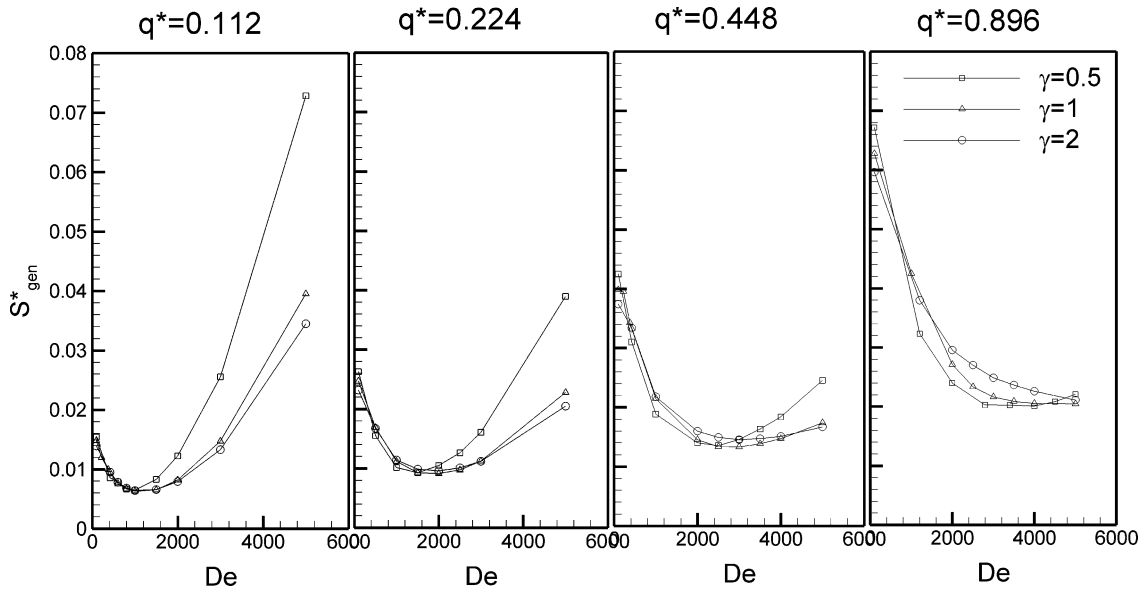

Fig. 14. The relationship between entropy generation, S'''_{gen}, and De for different aspect ratio cases with various q^*.

Table 1
Optimal aspect ratio for cases with different q^* and De

q^*	De	γ_{opt}
0.112	$De < 1000$	influence of γ is minor
	$1000 < De < 5000$	2
0.224	$De < 500$	2
	$500 < De < 1500$	0.5
	$1500 < De < 5000$	2
0.448	$De < 500$	2
	$500 < De < 2000$	0.5
	$2000 < De < 4000$	1
	$4000 < De < 5000$	2
0.896	$De < 680$	2
	$680 < De < 4000$	0.5
	$4000 < De < 5000$	1

cal distribution of the entropy generation, the larger S'''_{gen} region concentrates near the duct wall, where the temperature and velocity gradients are most serious. In the region near the heated outer wall, the entropy generation caused by heat transfer irreversibility is larger than that from the frictional irreversibility, and *verse vice* in the region near the inner wall. As the evaluation for the whole domain, the major source of entropy generation in the flow fields with larger De and smaller q^* comes from the frictional irreversibility, denoted by S^*_P; meanwhile for the flow fields with smaller De and larger q^* the entropy generation is dominated by the heat transfer irreversibility, denoted by S^*_T. The increase of q^* tends to cause the decrease of S^*_P and the increase of S^*_T. The competition between S^*_P and S^*_T is complicatedly related with De, q^* and γ, making the relationship between S^*_{gen} and q^*, and the relationship between S^*_{gen} and q^* non-monotonous. The optimal aspect ratio, γ_{opt}, with which the minimal entropy generation can be obtained, is dependent

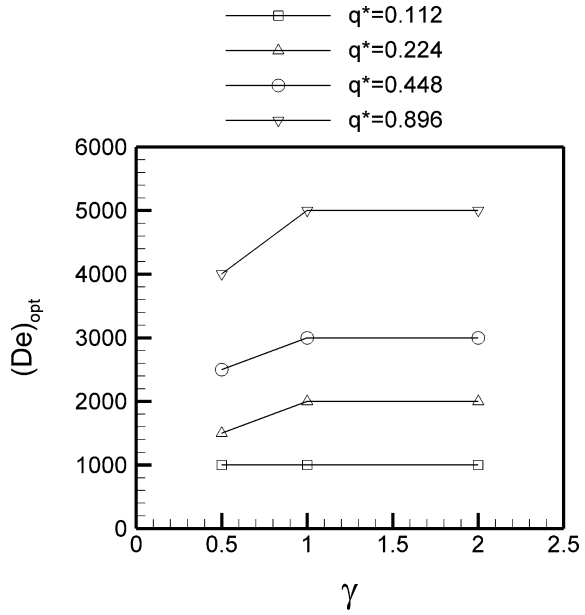

Fig. 15. The relationship between optimal De and γ for cases with different q^*.

on q^* and De. For each aspect ratio case, there exists an optimal De to induce the minimal S^*_{gen}, and the optimal De is found to increase as q^* increases. These results provided in the present paper are worthwhile for the heat exchanger design since the thermal system could have the least irreversibility and best exergy utilization if the optimal De and aspect ratio can be selected according to the practical design conditions.

References

[1] H. Ito, Flow in curved pipes, JMSE Internat. J. 30 (1987) 543–552.

[2] Z.F. Dong, M.A. Ebadian, Numerical analysis of laminar flow in curved elliptic ducts, J. Fluid Engrg. 113 (1991) 555–562.
[3] K.C. Cheng, J. Nakayama, M. Akiyama, Effect of finite and infinite aspect ratios on flow patterns in curved rectangular channels, in: Flow Visualisation, Tokyo, Japan, 1977, pp. 181–186.
[4] C.J. Bolinder, B. Sunden, Numerical prediction of laminar flow and forced convective heat transfer in a helical square duct with a finite pitch, Internat. J. Heat Mass Transfer 39 (15) (1996) 3101–3115.
[5] L. Wang, Buoyancy-force-driven transition in flow structures and their effects on heat transfer in a rotating curved channel, Internat. J. Heat Mass Transfer 40 (2) (1997) 220–235.
[6] R.J. Silva, R.M. Valle, M. Ziviani, Numerical hydrodynamic and thermal analysis of laminar flow in curved elliptic and rectangular ducts, Internat. J. Therm. Sci. 38 (1999) 585–594.
[7] T.T. Chandratilleke, Secondary flow characteristics and convective heat transfer in a curved rectangular duct with external heating, in: Proc. of 5th World Conference on Experimental Heat Transfer, Fluid Mechanics and Thermodynamics, ExHFT-5, Thessaloniki, Greece, September 24–28, 2001.
[8] T.T. Chandratilleke, Nursubyakto, Numerical prediction of secondary flow and convective heat transfer in externally heated curved rectangular ducts, Internat. J. Therm. Sci. 42 (2003) 187–198.
[9] A. Bejan, Entropy Generation Minimization, CRC Press, Boca Raton, FL, 1996.
[10] A. Bejan, Entropy Generation Through Heat and Fluid Flow, Wiley, New York, 1982.
[11] P.K. Nag, N. Kumar, Second law optimization of convection heat transfer through a duct with constant heat flux, Internat. J. Energy Res. 13 (1989) 537–543.
[12] A.Z. Sahin, Irreversibilities in various duct geometries with constant wall heat flux and laminar flow, Energy 23 (6) (1998) 465–473.
[13] A.Z. Sahin, Thermodynamics of laminar viscous flow through a duct subjected to constant heat flux, Energy 21 (12) (1996) 1179–1187.
[14] S.Z. Shuja, Optimal fin geometry based on exergoeconomic analysis for a pin-fin array with application to electronics cooling, Exergy 2 (2002) 248–258.
[15] O.N. Sara, S. Yapici, M. Yilmaz, T. Pekdemir, Secondary law analysis of rectangular channels with square pin-fins, Internat. Comm. Heat Mass Transfer 28 (5) (2001) 617–630.
[16] T.H. Ko, K. Ting, Entropy generation and thermodynamic optimization of fully developed laminar convection in a helical coil, Internat. Comm. Heat Mass Transfer 32 (2005) 214–223.
[17] T.H. Ko, K. Ting, Optimal Reynolds number for the fully developed laminar forced convection in a helical coiled tube, Energy (2005), submitted for publication.
[18] T.H. Ko, Y.C. Lin, K. Ting, Laminar forced convection and entropy generation in a helical coil with constant wall heat flux, Internat. J. Heat Mass Transfer (2005), submitted for publication.
[19] P.S. Srinivasan, Pressure drop and heat transfer in coils, Chem. Engrg. (1968) 113–119.
[20] P. Mishra, S.N. Gupta, Momentum transfer in curved pipes. 1. Newtonian fluids, Indust. Eng. Chem. Process Des Dev. 18 (1) (1979).
[21] S. Paoletti, F. Rispoli, E. Sciubba, Calculation of exergetic losses in compact heat exchanger passages, ASME AES 10 (1989) 21–29.
[22] B.E. Launder, D.B. Spalding, The numerical computation of turbulent flows, Comput. Methods Appl. Mech. Engrg. 3 (1974) 269–289.
[23] S.V. Patankar, Numerical Heat Transfer and Fluid Flow, Hemisphere, Washington, DC, 1980.